JACS
JOURNAL OF THE AMERICAN CHEMICAL SOCIETY
Article
pubs.acs.org/JACS

Formation of Nets of Corner-Shared Bicapped Gold Squares in $SrAu_3Ge$: How a $BaAl_4$-Type Derivative Reconciles Fewer Valence Electrons and the Origin of Its Uniaxial Negative Thermal Expansion

Qisheng Lin and John D Corbett*

Department of Chemistry, Iowa State University, Ames, Iowa 50011, United States

Supporting Information

ABSTRACT: $SrAu_3Ge$ was synthesized by direct fusion of the mixed elements at high temperature followed by annealing treatments, and its structure was determined by single crystal X-ray diffraction means in space group (Pearson symbol: *tP*10) *P*4/*nmm*, a = 6.264(1) Å, c = 5.5082(9) Å, Z = 2 at room temperature. The structure of $SrAu_3Ge$, a reapportioned $\sqrt{2} \times \sqrt{2} \times 1$ superstructure of $CeMg_2Si_2$ (*P*4/*mmm*), exhibits checkerboard nets of corner-shared bicapped Au squares (or corner-shared $Au(Au_{4/2})Ge$ octahedra), in which the apical Au−Ge pairs in adjoining nets are strongly interbonded in the c direction. This motif contrasts with that of the common $BaAl_4$ (*I*4/*mmm*) prototype in which Al squares in comparable layers are alternately monocapped by Al from the top or the bottom. Typical examples show valence electron counts (vec) between 12 and 16 for the $BaAl_4$ type and that for $CeMg_2Si_2$ is similar, 15. The special stability of SrAu3Ge, with vec = 9, derives from significant relativistic contribution of the Au $5d^{10}$ states to the Au−Ge and Au−Au bonding. These factors are also recognized in the marked redistribution of Au and Ge site occupancies from those in $CeMg_2Si_2$. $SrAu_3Ge$ exhibits a pronounced uniaxial negative thermal expansion along c, with a coefficient of −1.57 versus 2.16×10^{-5} K^{-1} in a and b. The reticulated Au_5Ge octahedral layers expand in the *ab* plane on heating, whereas the strong, interlayer Au−Ge bonds remain fixed.

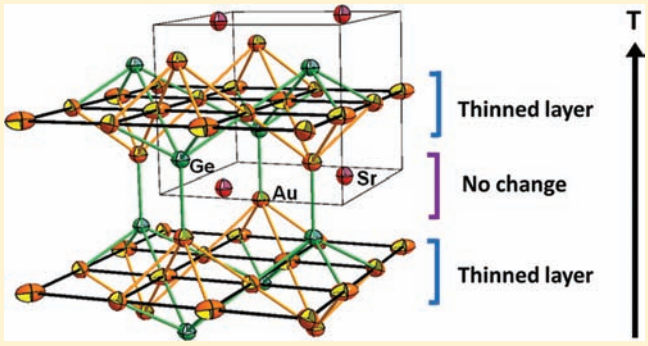

INTRODUCTION

Our extended searches for new quasicrystals (QC) and their neighboring approximant crystals (AC) gave us a valuable bonus when we studied the Ca−Au−Ga system:[1,2] not only an icosahedral QC and two conventional AC phases, but also the closely related 1/0 $CaAu_3Ge$ ($Pa\bar{3}$, a = 9.10 Å). The latter is the structurally simplest cubic approximant and a mimic of icosahedral QC models. The structure features two interpenetrating networks of three-dimensional (slightly distorted) Penrose Tiles that are defined by electropositive Ca and by electronegative Au and Ga atoms, respectively.

To this point, we imagined that chemical and electronic tunings of other possible isotypic phases might serve as suitable starting points for chemical tunings to new QCs and high-order ACs, in parallel to the results with Mg_2Zn_{11} type precursors.[3−5] A check of the literature revealed that $NaAu_3Si$ and $NaAu_3Ge$[6] are the only phases isostructural with $CaAu_3Ga$; moreover, each has a neighboring Bergman type 1/1 AC ($Na_{52}Au_{81}Si_{29}$ and $Na_{60}Au_{80}Ge_{30}$) in their respective phase fields.[7] These facts greatly encouraged us to seek other novel examples. Note also that this type of structure is not limited to the Au-rich compounds. The recent discovery of isostructural $AgPd_3Se$[8] illustrates that great opportunities exist for electronic tuning of other 1−3−1 phases.

Our first explorations examined the Au-rich phases $AeAu_3Tr$ with Ae = Ca, Sr, Ba, and Tr = Ge, Sn. These yielded exciting results, including not just the expected product $CaAu_3Ge$,[9] but also the unexpected $Ca_{14}Au_{45}Sn_6$,[10] $SrAu_3Ge$, $Sr_3Au_8Sn_3$,[9] and Ba_2Au_8Sn.[9] Presented here are the synthesis, structure, and bonding of $SrAu_3Ge$, which shows close relationships with its parents $CeMg_2Si_2$ and, further, $BaAl_4$ (and other ordered variants).[11] From the valence electron counts (vec) viewpoint, the contrasting $CeMg_2Si_2$ structure has been well explained as a preferred model for electron-rich $BaAl_4$-related derivatives (vec ≥ 16).[12] However, La_3Al_{11} type structures and its variants have usually been the preferred options for products with 12 or fewer electrons.[13] The structure of $SrAu_3Ge$ represents a new model with a compact unit cell and a low vec.

Surprisingly, $SrAu_3Ge$ also shows large uniaxial negative thermal expansion (NTE) in c, larger than that of the well-known NTE material ZrW_2O_8.[14] NTE materials are useful in systems subject to large temperature variations, such as telescope mirrors, thermo-mechanical actuators, tooth fillings, and other materials for which a fixed shape and size are desirable over a wide range of temperature. The uniaxial NTE behavior of $SrAu_3Ge$ may shed new light in the design and

Received: December 13, 2011
Published: February 21, 2012

dx.doi.org/10.1021/ja211625w | *J. Am. Chem. Soc.* 2012, 134, 4877−4884

exploitation of other NTE materials, including a reinvestigation of $CeMg_2Si_2$. The simple structure of $SrAu_3Ge$, with only four independent atoms in a unit cell, also may be a great playground for further study of NTE in theory.[15]

EXPERIMENTAL SECTION

Synthesis. All manipulations were performed in a N_2-filled glovebox (H_2O < 0.1 ppmv). Stoichiometric amounts of dendritic Sr pieces (99.95%, Alfa Aesar), with surfaces manually cleaned by a surgical blade, as-received Au particles (99.999%, Ames Lab), and Ge pieces (99.999%, Alfa Aesar) were weld-sealed into precleaned Ta containers ($\phi \approx 0.9$ cm) under Ar. The containers were then enclosed in evacuated SiO_2 jackets ($<10^{-5}$ Torr). $SrAu_3Ge$ was achieved in high yield (>85 vol %) by fusion of stoichiometric mixtures, ~ 400 mg in total, at 700 °C for 6 h, followed by cooling to 400 °C at a rate of 2 °C/h, annealing there for 6 d, and quenching into water. Reactions of $SrAu_{3+x}Ge_{1-x}$ ($x = \pm 0.5$) yielded mixtures with $SrAu_5$, $SrAu_2Ge_2$, and so forth as impurities, but the refined lattice parameters (below) indicated that the title phase was close to a line compound. $SrAu_3Ge$ is stable in air at room temperature for extended periods, and down to 110 K (see below).

Phase Analyses. These were performed on the basis of powder diffraction data collected by a Huber 670 Guinier powder camera equipped with an area detector and Cu Kα_1 radiation (λ = 1.540598 Å). The detection limit of a second phase with this instrument and system is conservatively estimated to be about 5 vol % in equivalent scattering power. Phase identifications were done with the aid of calculations from PowderCell,[16] and lattice parameters were refined with the aid of the program UnitCell[17] from data for at least seven reflection peaks between 16 and 60° in 2θ that were distinguishable from peaks of other phases. The refined lattice parameters for $SrAu_3Ge$ in $SrAu_{3+x}Ge_{1-x}$ products from reactions with x = −0.5, 0, and 0.5 fell in the range of a = 6.2798 (4)−6.2829(4) Å, c = 5.4948 (8)−5.4987 (8) Å, with maximum differences of ~5.5 and ~3.5 σ in a and c, respectively. Thus, $SrAu_3Ge$ appears to have an extremely small phase width.

SEM-EDX. Elemental compositions were determined via semi-quantitative energy-dispersive X-ray spectroscopy (EDX) on a JEOL 59101v scanning electron microscope (SEM). Samples were mounted in epoxy, carefully polished, and then sputter-coated with a thin layer of carbon prior to loading into the SEM chamber. Accelerating voltage of 20 K eV was used. Samples were first scanned by means of backscattered electrons, through which different phases could be seen in regions with different darknesses. Elemental proportions for selected single-phase areas were then measured. The average of four readings from a nominal $SrAu_3Ge$ sample was Sr/Au/Ge = 1:3.0(1):1.0(1) relative to the Sr content. These proportions are consistent with the more precise compositions refined from single crystal X-ray diffraction data.

Structure Determination. Selected single crystals were mounted on a Bruker APEX CCD single crystal diffractometer equipped with graphite-monochromatized Mo Kα (λ = 0.71069 Å) radiation. Intensity data were collected in an ω scan mode over 2θ = ~ 7−57° and with exposures of 30 s per frame. Data sets at room temperature (295 K), 173 K, and 110 K were collected from the same crystal. The lattice parameters refined from all observed reflections were a = 6.2741 (10) Å, c = 5.4944 (9) Å at 295 K; a = 6.2638 (10) Å, c = 5.5082 (9) Å at 173 K; and a = 6.2490 (9) Å, c = 5.5104 (8) Å at 110K. The reflections in all data sets were consistent with the primitive tetragonal 4/m symmetry. Data integration, Lorentz polarization, and other corrections were made by SAINT subprogram included in the SMART software package.[18] Empirical absorption corrections were performed with the aid of the subprogram SADABS. Systematic analyses in SHELXTL indicated two possible centric space groups for the first two data sets: $P4/n$ and $P4/nmm$, but the former symmetry was excluded after additional mirror planes were suggested by the program Platon.[19]

For the room temperature data, direct methods in the $P4/nmm$ model yielded all four independent atom sites. Of these, three had suitable distances for Au/Ge−Au/Ge contacts, and one for Sr−Au/Ge contacts. Therefore, the former three were temporarily assigned to Au1−Au3 and the other, to Sr. Subsequent refinements converged at R1 ≈ 13.7%. At this stage, the isotropic displacement parameter for one of the three sites assigned to Au was about 7 times the average of the others (0.090 versus 0.013 Å^2), suggesting a site for Ge, a Au/Ge mixture, or with fractional occupancy. Assignment of Ge to this produced normal isotropic parameters (0.015−0.021 Å^2) for all atoms and a drastically decreased R1 (7.2%). The site occupancies were then separately refined, but all fell well within 1 σ of unity, that is, 0.99(4)−1.00(2). The composition calculated with such assignments was $SrAu_3Ge$, agreeing with the more approximate EDX data. The final refinements with anisotropic displacement parameters yielded R1 = 2.77%, wR2 = 5.74%, and GOF = 1.13 for 13 parameters refined from 177 observed independent reflections. The maximum peak and hole in the difference map were 1.67 and −4.04 e/Å^3, respectively, both within 1.21 Å from Ge.

It should be noted that Au1 has the largest isotropic displacement parameters in the structure (0.022 Å^2), about 50% larger than the average for the other atoms. The anisotropic displacement parameters revealed that Au1 has elongated ellipsoids in the ab plane (below). This feature is not the result of a wrong atom assignment (above), poor absorption corrections, or poor crystal quality inasmuch as another crystal yielded the same trend. Although such behavior might instead be attributed to an incipient phase transition, the feature remains unchanged after lower temperature X-ray diffraction analyses (below). Twinning in a $P4/n$ model as a source of the behavior was ruled out inasmuch as the same dispositions remain on such a refinement. The presence of the additional mirror symmetry in $P4/nmm$ was also established. Rather, the effects are caused by the special geometry of Au_5Ge octahedral clusters and the bonding between them, which will be discussed later.

The results for the 110 and 173 K data set are very similar to those of 295 K. As expected, the displacement parameters at lower temperatures are systemically smaller. The crystallographic data and structure refinements for all three temperatures are summarized in Table 1, and the refined positional and isotropic-equivalent displacement parameters, in Table 2. The anisotropic displacement parameters are also given in Table 3 to demonstrate the regularities of the system, and the important interatomic distances are listed in Table 4 together with corresponding −ICOHP values. Detailed crystallographic data are available in the cif outputs (Supporting Information).

Table 1. Crystal and Structural Refinement Data for $SrAu_3Ge$ at Different Temperatures

temp	110 K	173 K	295 K
f.w.	751.11	751.11	751.11
Space group, Z	$P4/nmm$, 2	$P4/nmm$, 2	$P4/nmm$, 2
unit cell (Å)			
a	6.2490(9)	6.264(1)	6.274(1)
c	5.5104(8)	5.5082(9)	5.4944(9)
Vol. (Å^3), d_{cal} (g/cm^3)	215.18(5), 11.593	216.12(6), 11.542	216.28(6), 11.533
data/restr./para.	175/0/14	174/0/13	177/0/13
GOF on F^2	1.209	1.223	1.128
R1/wR2 [$I > 2\sigma(I)$]	0.0214/0.0483	0.0223/0.0499	0.0277/0.0574
(all data)	0.0223/0.0485	0.0284/0.0511	0.0326/0.0560
diff. peak/hole (eÅ^{-3})	1.96/−2.03	2.01/− 1.97	1.67/− 4.04

Electronic Structure Calculations. The calculations were performed by means of the self-consistent, tight-binding, linear-muffin-tin-orbital (LMTO) method in the local density (LDA) and atomic sphere (ASA) approximations, within the framework of the DFT method.[20−23] ASA radii were scaled at the limit of 18% maximum overlap between two neighboring atomic spheres, and no interstitial sphere was necessary. The ASA radii for Sr, Au1, Au2, and Ge were about 4.39, 2.89, 2.89, and 2.57 Å, respectively. Reciprocal space

Table 2. Atomic Coordinates and Isotropic Equivalent Displacement Parameters for $SrAu_3Ge$ at 110, 173, and 295 K[a]

atom	Wyck.	symm.	x	y	z	Ueq (Å^2)[b]
Au1	4*e*	4*mm*	0	1/2	1/2	0.011(1)
			0	1/2	1/2	0.016(1)
			0	1/2	1/2	0.022(1)
Au2	2*c*	..*m*	1/4	1/4	0.8198(2)	0.010(1)
			1/4	1/4	0.8204(2)	0.012(1)
			1/4	1/4	0.8213(2)	0.015(1)
Ge	2*c*	..*m*	1/4	1/4	0.2656(5)	0.008(1)
			1/4	1/4	0.2665(5)	0.010(1)
			1/4	1/4	0.2683(5)	0.013(1)
Sr	2*a*	..2/*m*	1/4	3/4	0	0.008(1)
			1/4	3/4	0	0.011(1)
			1/4	3/4	0	0.015(1)

[a]The data for 110, 173, and 295 K are listed in sequence. [b]Ueq is defined as one-third of the trace of the orthogonalized U_{ij} tensor.

Table 3. Refined Anisotropic Displacement Parameters ($\times 10^3$ Å^2) for $SrAu_3Ge$ at 110, 173, and 295 K[a,b]

atom	U_{11}	U_{33}	U_{23}	U_{13}	U_{12}
Au1	14(1)	6(1)	0(1)	0(1)	6(1)
	19(1)	10(1)	0(1)	0(1)	9(1)
	24(1)	17(1)	0(1)	0(1)	13(1)
Au2	11(1)	6(1)	0	0	0
	13(1)	10(1)	0	0	0
	16(1)	14(1)	0	0	0
Ge	8(1)	7(1)	0	0	0
	11(1)	9(1)	0	0	0
	13(1)	12(1)	0	0	0
Sr	9(1)	6(1)	0	0	0
	11(1)	12(1)	0	0	0
	12(1)	19(2)	0	0	0

[a]The data for 110, 173, and 295 K are listed in sequence. [b] $U_{22} = U_{11}$.

integrations were carried out by means of the tetrahedron method. The basis sets were 4d/5s/(5p) for Sr, 5d/(5f)/6s/6p for Au, and 4s/4p/(4d) for Ge, with orbitals in parentheses down-folded.[24] Scalar relativistic effects were included in the calculations. The band structure was sampled for 24 × 24 × 24 k points in the irreducible wedge of the Brillouin zone. Crystal orbital Hamilton population (−COHP)[25] analyses were also performed to gain insights into the bonding properties.

The molecular orbital analyses for the Au_4 square, the Au_5Ge octahedron, and their combination were performed using the semiempirical extended-Hückel tight-binding (EHTB) method via CAESAR.[26] The orbital energies (H_{ii}) and Slater exponents (ζ) employed in the calculation were:[26] Au 6s, H_{ii} = −10.92 eV, ζ_1 = 2.602, c_1 = 1.0; 6p, H_{ii} = −5.55 eV, ζ_1 = 2.584, c_1 = 1.0; 5d, H_{ii} = −15.076 eV, ζ_1 = 6.163, c_1 = 0.6851, ζ_2 = 2.794, c_1 = 0.5696. Ge 4s, H_{ii} = −16.0 eV, ζ_1 = 2.16, c_1 = 1.0; 6p, H_{ii} = −9.0 eV, ζ_1 = 1.85, c_1 = 1.0.

RESULTS AND DISCUSSION

Structure. $SrAu_3Ge$ crystallizes in space group *P*4/*nmm* (Pearson symbol *tP*10), with $a = \sqrt{2}a_0$, $c = (1/2)c_0$, in which a_0 and c_0 denote the lattice parameters of the parent tetragonal $BaAl_4$ (*I*4/*mmm*). This structure is isostructural with $BaAu_3Ge$, the structure of which was recently reported without further comment.[27] $SrAu_3Ge$ exhibits some close relationships with $BaAl_4$ and its ordered ternary structure types ($ThCr_2Si_2$, $CaBe_2Ge_2$, and $BaNiSn_3$)[11] and particularly, the primitive $CeMg_2Si_2$ in terms of structural motifs. Nonetheless, $SrAu_3Ge$ is a notable electron-poor derivative of $BaAl_4$ (*P*4/*nmm*) and its progeny. Crystallographically, $SrAu_3Ge$ (Z = 2) is a reapportioned $\sqrt{2} \times \sqrt{2} \times 1$ superstructure of $CeMg_2Si_2$ (*P*4/*mmm*, Z = 1),[28] in which Ce occupies the Wyckoff 1*a* (0 0 0), Mg occupies 2*e* (0 $^1/_2$ $^1/_2$), and Si occupies 2*h* ($^1/_2$ $^1/_2$ z) sites, as detailed in Figure 1. Although the conversion to $SrAu_3Ge$ reflects straightforward crystallographic relationships, the chemical alterations suggest major differences. The former Wyckoff 2*h*

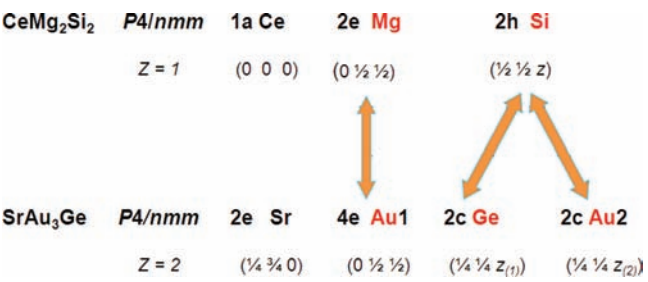

Figure 1. The crystallographic and atom site relationships between $SrAu_3Ge$ and its parent $CeMg_2Si_2$. The chemical alternations between them are impressive (colored arrows).

Si site in *P*4/*mmm* gives rise to two 2*c* sites in *P*4/*nmm* that are now occupied by the contrasting Au2 and Ge, respectively, whereas the former 2*e* Mg site is converted to

Table 4. Important Interatomic Distances (Å) at 110, 173, and 295 K, the Difference (Δd) between 110 and 295 K data, and −ICOHP (eV/bond·mol) Values for $SrAu_3Ge$[a]

bond	multi.	dist. (Å)	Δd (Å)	−ICOHP	bond	multi.	dist. (Å)	Δd (Å)	−ICOHP
Au1−Ge	4	2.559(1)			Au2−Ge	2	3.053(3)		
		2.561(1)					3.051(3)		
		2.558(1)	−0.001(1)	2.35			3.038(3)	−0.015(4)	0.34
Au1−Au2	4	2.8259(7)			Sr−Au1	16	3.5316(3)		
		2.8319(7)					3.5340(4)		
		2.8349(7)	0.009(1)	1.28			3.5310(4)	−0.0006(5)	0.36
Au1−Au1	8	3.1245(5)			Sr−Au2	8	3.2786(5)		
		3.1319(5)					3.2844(6)		
		3.1370(5)	0.0125(7)	0.70			3.2871(6)	0.0085(8)	0.43
Au2−Ge	2	2.457(3)			Sr−Ge	8	3.450(1)		
		2.457(3)					3.459(1)		
		2.456(3)	−0.001(4)	2.96			3.466 (1)	0.016(1)	0.41

[a]The data for 110, 173, and 295 K are listed in sequence.

dx.doi.org/10.1021/ja211625w | J. Am. Chem. Soc. 2012, 134, 4877−4884

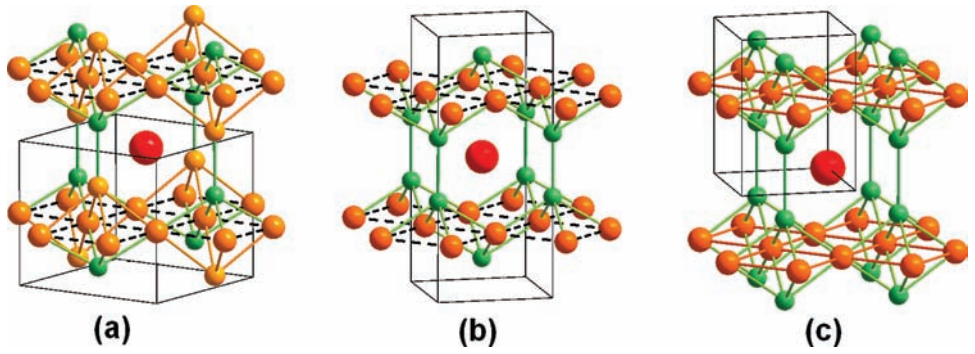

Figure 2. Comparison of structural motifs among (a) $SrAu_3Ge$, (b) $SrAu_2Ge_2$ ($ThCr_2Si_2$ type), and (c) $CeMg_2Si_2$. Notice also the different unit cell proportions. Gold spheres represent Au; green, Ge; and red, Sr in (a) and (b) and Mg, Si, and Ce, respectively in (c).

4e Au1 atoms. These redistributions of apparent atom polarities and, especially, the addition of $5d^{10}$ bonding contributions of gold are noteworthy (below). Even so, the space groups of both $SrAu_3Ge$ and $CeMg_2Si_2$ are maximum *Klassengleiche* subgroups of that of $BaAl_4$ ($I4/mmm$).

Figure 2a shows the extended structure of $SrAu_3Ge$, with the unit cell outlined with solid black lines. The Au1 atoms are equally spaced and form a two-dimensional basal square net at $z = 1/2$ (dashed). The last feature is a characteristic structural motif of the well-known $BaAl_4$ prototype and its subtypes, $ThCr_2Si_2$, $CaBe_2Ge_2$, and $BaNiSn_3$.[11] All $BaAl_4$ family members exhibit square pyramidal layers in which the basal square nets are alternately capped from above and below, as shown in Figure 2b for the equivalent ternary $SrAu_2Ge_2$ ($ThCr_2Si_2$-type).[29,30] Such square pyramidal layers appear as checkerboards if the top-capped square nets are deemed as "black" and the bottom-capped as "white", or vice versa. In comparison, the basal square nets in $SrAu_3Ge$ show a different feature: one-half of the squares are trans-bicapped by apical Au2 and Ge to form Au_5Ge octahedra, whereas the remaining squares lie opposite Sr cations. The two sets of squares again define a checkerboard pattern, similar to that in $SrAu_2Ge_2$, but the octahedra themselves generate a second-order checkerboard pattern in consideration of their "polar" character, as shown by the dashed red lines in Figure 3. This is the reason the lattice parameter a is increased to $\sqrt{2}a_0$.

The remarkable layers in $SrAu_3Ge$ can also be viewed as corner-shared "polar" Au_5Ge octahedra with alternating trans-configurations along c (see Figures 2a and 3). In comparison, corner-shared Mg_4Si_2 octahedra in $CeMg_2Si_2$ are nonpolar (Figure 2c). In three dimensions, neighboring basal layers in the present example are interlinked through the apical-to-apical Au2−Ge bonds, the shortest in the structure. This results in the formation of large cavities defined by 8 Au1, 4 Au2, and 4 Ge atoms that are customarily occupied by the counter-cationic Sr at ($^1/_2$ $^1/_2$ 0). Note that these cavities are exactly sandwiched by two empty squares in the basal layers in the c direction. In contrast, the parallel cavities in $SrAu_2Ge_2$ are sandwiched by two square pyramids, thus, adding two additional and more distant capping atoms around Sr and along c, Figure 2b.

As listed in Table 4, the basal-to-apical contacts in $SrAu_3Ge$ at room temperature are 2.835 (1) Å and 2.558 (1) Å for $d_{Au1-Au2}$ and d_{Au2-Ge}, respectively. The latter is ∼0.07 Å less than the parallel interaction in $SrAu_2Ge_2$ (2.628 Å). However, the basal-to-basal distance ($d_{Au1-Au1}$ = 3.137 Å) is about 0.04 Å larger than that in $SrAu_2Ge_2$. From another viewpoint, each $(Au1)_4Ge$ pyramid in $SrAu_3Ge$ is relatively expanded in the

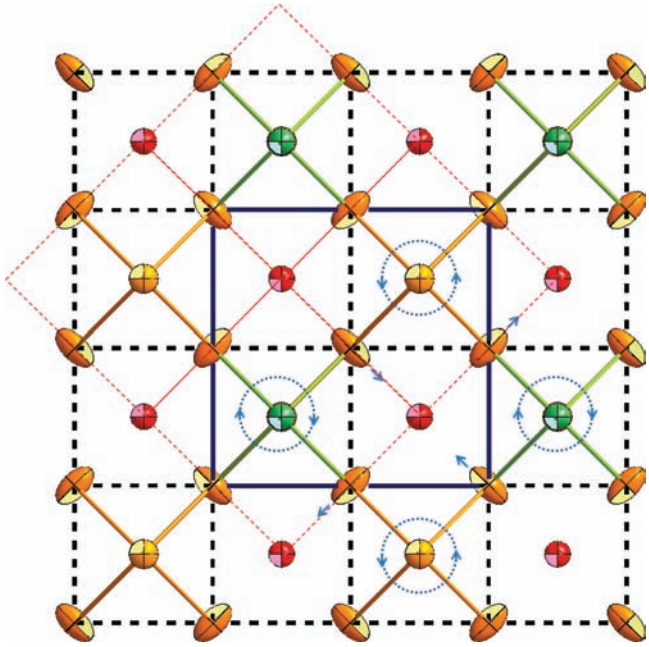

Figure 3. The (001) projection of 4 × 4 squares (dashed black) in $SrAu_3Ge$, with atoms represented by ellipsoids drawn at 95% probability (295 K). A unit cell is highlighted by solid black lines. Squares marked by dashed red lines denote the second-order checkerboard (cf. text), and arrows indicate the possible choices for the motion of octahedra. Gold ellipsoids represent Au (two types); green, Ge; and red, Sr atoms.

$a-b$ plane or compressed along c compared with that in $SrAu_2Ge_2$. The smaller intralayer distance within each octahedron, d_{Au2-Ge} = 3.038(4) Å, is one of the additional characteristics. The interlayer Au2−Ge bond in $SrAu_3Ge$ is, surprisingly, about 0.06 Å *shorter* than the interlayer Ge−Ge bond in $SrAu_2Ge_2$ (2.456(3) versus 2.494(4) Å). This distance is even about 0.1 Å less than the sum of the covalent radii of Au and Ge (Au, 1.36 Å; Ge, 1.20 Å) from Alvarez,[31] a signature of strong covalent bonding. Nevertheless, slightly shorter Au−Ge bonds occur in the isolated molecular-like cluster $(Au_3Ge_{18})^{5-}$ in the $[K([2.2.2]crypt)]_{15}[Au_3Ge_{18}]$ salt, ∼ 2.437−2.460 Å, in which the coordination number of gold is lower.[32]

It should be noted that the basal Au1 atoms in $SrAu_3Ge$ always exhibit elongated anisotropic ellipsoids in the $a-b$ plane. The same is true in the isostructural $BaAu_3Ge$, in which the larger cation also leads to further expansion of both $d_{Au1-Au1}$ in the basal layers and the interlayer d_{Au2-Ge}.[27] In contrast, no

dx.doi.org/10.1021/ja211625w | J. Am. Chem. Soc. 2012, 134, 4877−4884

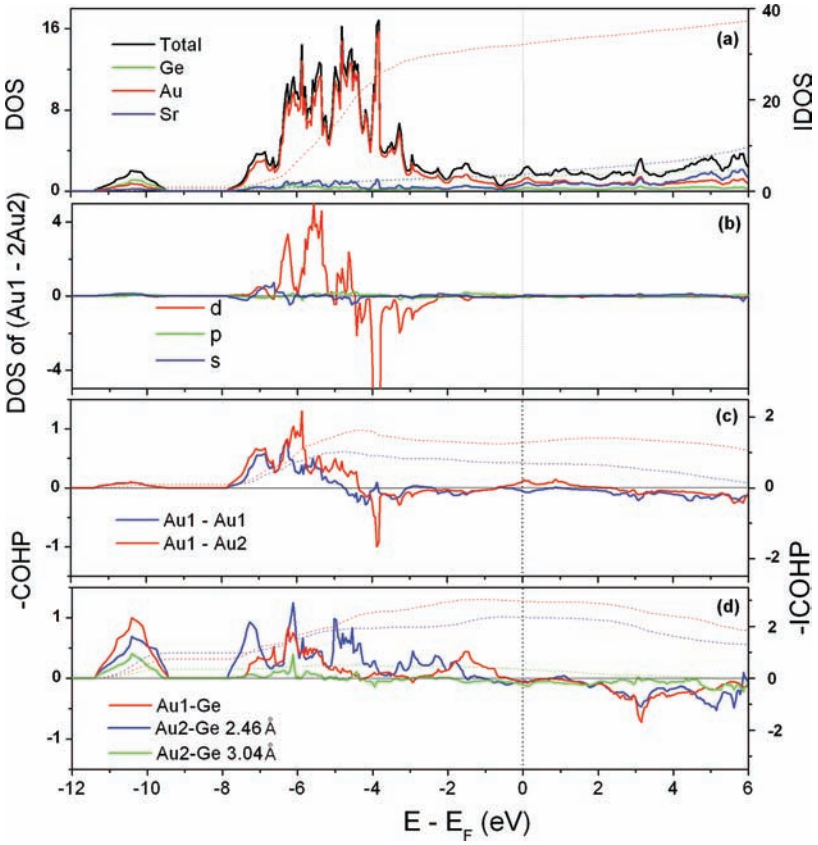

Figure 4. (a) The total and projected density-of-states (eV/formula) and integrated DOS (dotted) for $SrAu_3Ge$. (b) The *difference* in DOS for Au1 and Au2. (Note the correction for the Au1/Au2 = 2:1 proportion). (c) The crystal orbital Hamilton population (−COHP) data (eV/bond) for Au1−Au1 and Au1−Au2 bonds and (d) for Au1−Ge and both interlayer and intralayer Au2−Ge bonds in $SrAu_3Ge$. Dashed lines in (c) and (d) are integrated −COHP data for corresponding colored −COHP curves.

atom in $SrAu_2Ge_2$ shows a particularly elongated displacement parameter (Supporting Information Table S1). We believe that the elongation of Au1 ellipsoids is associated with the compression of the octahedral layer (above) and that this could continue at higher temperatures assuming that the shortening of the intralayer distance d_{Au2-Ge} remains. Whether a phase transition occurs at higher temperatures (>295 K) is beyond this study, but a future goal is to further characterize the negative thermal expansion property of $SrAu_3Ge$.

Electronic Structure. Figure 4a shows the total and projected densities-of-states (DOS) for each component in $SrAu_3Ge$ at room temperature. The DOS below −9.0 eV are dominated by Ge 4s and Au 6s states, which generate the head-to-head σ bonding. The large peaks between −8.0 and −3.0 eV are dominated by Au 5d states, together with some that originate from Au 6s, Ge 4p, and Sr 5s, 5p states (cf. Figure S1). The spiky character suggests complex interactions among these orbitals, including s−s, s−p, s−d, and p−p interactions of Au1−Ge and Au2−Ge, the s−s, s−p, s−d, p−p, p−d, and d−d interactions of Au1−Au1 and Au1−Au2, and those with Sr 5s and 5p. (For detailed orbital interactions, readers can refer to the eigenvectors given in Table S2.) The basal Au1 has larger contributions than Au2 below ca. − 4.5 eV; in parallel, the contribution from apical Au2 exceeds that from Au1 in the region between −4.5 and −2.0 eV, Figure 4b. (Note that the influence of the 2:1 proportion for Au1/Au2 has been considered.) This fact is consistent with their different roles in the structure. On the other hand, the influence of Au $5d^{10}$ on the Fermi surface is very small, as indicated by fatband analyses (Figure S2). Therefore, $SrAu_3Ge$ might still be simply considered an s−p bonded compound in electron counting, as for other $BaAl_4$ derivatives,[33] but the bonding is substantially perturbed by Au $5d^{10}$ contributions at lower energies. As expected from the bond distances, the Au1−Ge, Au1−Au2, and Au2−Ge bonds show strong bonding character, Figure 4c,d. The bond indexes, evaluated as integrated −COHP (−ICOHP) data, Table 4, indicate that the largest bond populations in $SrAu_3Ge$ are Au2−Ge (2.96 eV/bond·mol), followed by the basal-to-apical Au1−Ge (2.35) and Au1−Au2 bond (1.28). Other interactions are at most one-fourth of the largest, although comparisons between different elements should not be taken too literally. These indicate that the Au_5Ge octahedra in $SrAu_3Ge$ are strongly bonded units that form octahedral chains along *c* in the structure.

Electron Counts in $SrAu_3Ge$, $BaAl_4$, and $CeMg_2Si_2$ Structures. As shown in Figure 2, the structures of $SrAu_3Ge$ and $CeMg_2Si_2$ are different from that of $SrAu_2Ge_2$ (and other $BaAl_4$-type ordered variants, viz., $CaBe_2Ge_2$ and $BaNiSn_3$), but all of these structural types have certain connections in terms of vec. The meaningful comparison among these 1:4 phases relies on the fact that they all exhibit common features of square nets.

It is well-known that the normal $BaAl_4$ type phases (including its ordered variants) are optimized near 14 vec per formula unit,[12] but this value is known to vary over ±2 because other factors (size, packing, bonding, etc.) also play pronounced roles in structural stabilization, for example, for $CaAu_2Si_2$ (12), $CaAuAl_3$ (12), RAl_2Ga_2 (R = rare-earth metal) (15), and $SrAl_2Pb_2$ (16).[34] Zheng and Hoffmann[12] have

dx.doi.org/10.1021/ja211625w | J. Am. Chem. Soc. 2012, 134, 4877−4884

demonstrated by means of EHTB bonding analyses that the $CeMg_2Si_2$ type structure is predicted to be more stable than the $BaAl_4$ type for typical analogues with large vec values ($\geq$15); vice versa, $BaAl_4$ structures are more stable than $CeMg_2Si_2$ at vec $\leq$ 15. Yet, no simple 1:4 phase has hitherto been reported in the lower vec region (<12). Rather, the La_3Al_{11} type superstructures and other substoichiometric variants are often observed as effective ways to circumvent a low vec, for example, K_3Hg11,[35] $Ca_3Au_8Ge_3$,[13] and La_2NiAl_7.[36] The only exception appears to be the recently reported isostructural $BaAu_3Ge$.[27]

Apparently, the present structural model of $SrAu_3Ge$, with 9 vec per formula (without counting the lower but nearby Au $5d^{10}$ in the valence shell) represents a preference for electron-poor phases, opposite to the related electron-rich $CeMg_2Si_2$ type and $BaAl_4$. In other words, formation of corner-shared bicapped squares in $SrAu_3Ge$ and its supposed parent $CeMg_2Si_2$ rather than edge-shared square pyramids (in $BaAl_4$ and its ordered variants) represent options for both electron-rich (vec $\geq$ 15) and electron-poor ($\leq$12) 1:4 phases. (Tetravalent cation substitutions in or other variations of the singular $CeMg_2Si_2$ to reach the 16-electron version have evidently not been tried, or successfully so, anyway.)

To account for the vec preference for $SrAu_3Ge$ and to make a straightforward comparisons with $BaAl_4$ and $CeMg_2Si_2$, we recall the rationale employed by Zheng and Hoffmann[12] regarding the electronic structures of these two. That is, the electronic structures of $BaAl_4$ and $CeMg_2Si_2$ types may be developed from two-dimensional layers of square nets that are differently capped by apical atoms. According to EHTB calculations, the electronic structure of a single layer in $BaAl_4$ contains eight low-lying bands per four Al, with two of these localized on the apical Al. On stacking in three dimensions, the formation of interlayer bonds pushes one of these up as σ^* band, thus, leaving seven bands in a strongly bonding region and nine in a strongly antibonding region. This is why and how a typical $BaAl_4$ type phase is considered to be optimized at vec = 14. Similar analysis of the 15-electron $CeMg_2Si_2$ reveals five bands in a strongly bonding region, five in a nonbonding region, and six that are strongly antibonding (cf. scheme 31 in ref 12). Thus, occupation of the first two groups yields a structural stabilization near vec of 20, whereas the observed 15-electron phase must then include the complication of "other effects". (Interested readers should refer to the 29-page ref 12 for detailed procedures.)

Figure 5 shows part of the corresponding orbital diagram for an Au_4 square, an Au_5Ge octahedron, and their combination. Excluding the Au 5d orbitals (−16.0 and −14.0 eV), these yield five orbitals in the strong bonding region (<−10 eV) and four (or five) orbitals in the nonbonding region (between −9.0 and −7.0 eV), about the same situation as that of $CeMg_2Si_2$ (above). The major differences are the degeneracies of hybridized orbitals in the bonding and nonbonding regions and, of course, the fact that the EHTB approach does not take relativistic effects for the Au d^{10} orbitals into account. However, extension of the bonding analysis to three dimensions by means of more quantitative LMTO methods shows the course of the interlayer bonding interactions with Au d^{10} as well as Sr. In particular, the −COHP data (Figure 4) show that five bands in strongly bonding region are fairly well separated from those in the nonbonding and antibonding regions, giving a preferred lower vec of 9 or 10. The crystallographic relationships between Wyckoff sites in space groups *P*4/*mmm* and *P*4/*nmm* carry no information regarding the intra- and intersite bonding. The

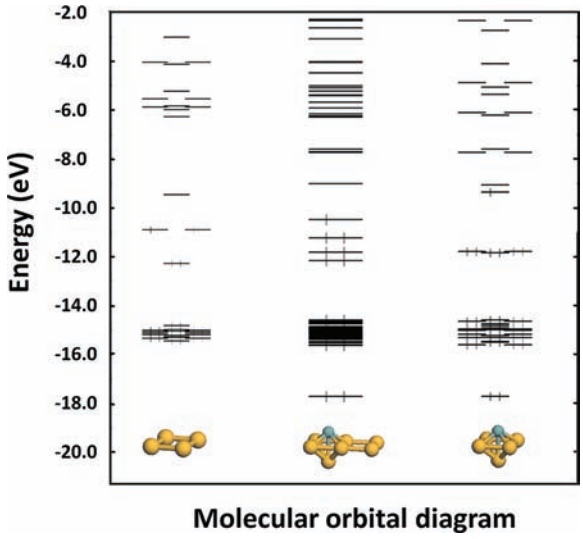

Figure 5. The molecular orbital diagram for a Au_4 square, a Au_5Ge octahedron, and their combination to generate a precursor of $SrAu_3Ge$.

contrary atom distributions, Figure 1, emphasize that chemistry and bonding in the two phases must be very different as well, and this must lie largely with the relativistic effects that are so important in many intermetallic phases of gold.[37,38]

Uniaxial Negative Thermal Expansion (NTE). According to single crystal X-ray diffraction analyses, the unit cell of $SrAu_3Ge$ expands by 0.025(1) Å in the *a* and *b* axes (the basal square nets) and contracts 0.016 (1) Å in *c* on heating from 110 to 295 K (Table 1). The calculated coefficients[39] of thermal expansion in *a* (*b*) and *c* are 2.16×10^{-5} K^{-1} and -1.57×10^{-5} K^{-1}, respectively, indicating that $SrAu_3Ge$ exhibits a large uniaxial NTE along *c*. (For reference, the NTE coefficient for ZrW_2O_8 is similar, about -9×10^{-6} K^{-1} over 0.3−1050 K.[14]) As expected, such divergent lattice variations can result in a very small change in the unit cell volume, only ~0.51% from 110 to 295 K.

NTE behavior may be incurred by different mechanisms, for example, by rigid unit modes, varying electronic configurations, magnetic ordering, and conduction electron or vibrational effects.[40] We believe that the NTE of $SrAu_3Ge$ is related to its particular geometry rather than other features. As a matter of fact, the anisotropic lattice changes in $SrAu_3Ge$ correspond well to the variations of related bond distances. That is, the in-plane Au1−Au1 distances in the basal square nets increase 0.0125(7) Å over the range studied, Table 3, one-half of the change of lattice parameter *a*. (Remember that each unit cell consists of 2 × 2 squares, Figure 2.) In the *c* direction, the 0.015(4) Å decrease of intralayer Au2−Ge distance within each octahedron, is indistinguishable from the change of the *c* lattice parameter, −0.016 (1) Å. In other words, the variation of the *c* lattice parameter is more germane to a compression of the octahedral layer than any shortening of the strong Au2−Ge interlayer bonds, which in fact shows negligible change (−0.001(4) Å) over the temperature range. A common NTE driving force is the so-called rigid unit mode, as observed in ZrW_2O_8,[41] ScF_3,[42] and ReO_3.[43] in which the rigid structural units (e.g., octahedra) pivot or rock relative to each other to reduce the total volume. Although the Au_5Ge octahedra in $SrAu_3Ge$ could presumably mimic similar pivot-and-rock motions (cf. Figure 2), as in ZrW_2O_8, the observed NTE

dx.doi.org/10.1021/ja211625w | *J. Am. Chem. Soc.* 2012, 134, 4877−4884

along *c* and the expansion in *ab* plane of $SrAu_3Ge$ (on heating) are more analogous to the release of a "squeezed frog". This change may be related to the different bond strengths within the Au_5Ge octahedra, as suggested by the −ICOHP data in Table 4. That is, the weaker basal-to-basal bonding allows a more normal change with as temperature, but the strong basal-to-apical bonds restrain atom motions along *c*. A uniaxial NTE effect is also observed in the hexagonal YbGaGe ($P6_3/mmc$) in which NTE in the *ab* plane and positive thermal expansion in *c* are apparently driven by the mixed Yb^{2+}/Yb^{3+} valency.[44]

FURTHER THOUGHTS

As we know, the $BaAl_4$ family represents one of the richest pools for technologically important materials in magnetic, heavy Fermion, and superconducting applications. The recent discovery of unconventional Fe-based superconductors[45] rebooted interest in new superconductive examples among the $BaAl_4$ type intermetallic compounds and their derivatives.[46,47] The magnetically active Fe atoms in the structure of AFe_2As_2 (A = Ca, Sr, Ba) occupy the so-called basal sites only, whereas the nonmagnetic As atoms lie in the more strongly bonded apical sites. However, these phases do not show superconductivity without doping (at normal pressure). It is believed that magnetic fluctuations in close proximity to a very energetic antiferromagnetic state induce superconductivity.[46] However, evidently no report regarding to the outcome of placing excess magnetically active centers on apical sites is available.

Apparently, a replacement of one-half of the apical atoms in $BaAl_4$ type structure by transition metals would result in a large change in vec. Whether vec is increased or decreased depends on how the valence electrons of transition metals are counted. (Unfortunately, this is a still unsolved question.) For example, people may prefer eight for the valency of Fe, but in many cases, particularly in magnetic materials, − 2.66 is the better value according to Pauling.[48,49] Nevertheless, both counting schemes should predict whether a $CeMg_2Si_2$ or a $SrAu_3Ge$ type structure or unknown variants form if no superlattice or intergrowth structure occur. On the other hand, intergrowth structures of a $SrAu_3Ge$-type phase and a magnetically active AFe_2As_2 (A = Ca, Sr, Ba) superconducting phase, if stable, could also be an interesting test of the influence of inter- and intralayer couplings on T_c.[50]

CONCLUSIONS

This work demonstrates that fascinating chemistries exist in electron-poor phase regions that are not limited to QC/ACs. Here, the structure and bonding of $SrAu_3Ge$, a structural type for electron-poorer $BaAl_4$ derivatives, has been examined. As a formal superstructure of $CeMg_2Si_2$, $SrAu_3Ge$ is vacancy-free and has a compact unit cell, comparable to that of $BaAl_4$, and the additional influence of Au on the bonding would appear to be substantial. The structures of $SrAu_3Ge$ and $CeMg_2Si_2$ represent two distinctive extremities that are suitable for $BaAl_4$ derivatives with smaller (≤10) or larger (≥15) vec values. The present structure may shed new light on chemical tuning with other transition metals, our future work. For example, the quest to make new examples with similar octahedral layers but exhibiting $CaBe_2Ge_2$ and $BaNiSn_3$-like ordering would be interesting. However, the choices of active metals and p-block metal combinations need additional considerations of orbital energies to meet the electronic structural requirements. In a more general sense, it has already become apparent that one-for-one substitutions of a single neighboring congener atom into a QC structure, or a prospect therefore, often leads to new and unexpected products that exhibit major changes in structure, as happened here.[51,52] Both atom packing and electronic fits appear to be very dependent on size and probably on other factors we do not yet appreciate.

$SrAu_3Ge$ shows large uniaxial NTE in *c*, whereas its basal *a* and *b* axes show positive responses. As a result, ∼ 0.51% change in unit cell volume is found between 110 and 295 K, suggesting a nearly zero thermal expansion (ZTE) material. Although $SrAu_3Ge$ contains rigid octahedra, the NTE in $SrAu_3Ge$ is evidently related to a rare motion of the reticulated Au_5Ge, in contrast to the pivot-and-rock motion as commonly seen in other NTE materials, for example, ZrW_2O_8[14,41] and ScF_3.[42] The unixial NTE behavior of $SrAu_3Ge$ may shed new light in the future design and exploitation of other NTE materials, including a reinvestigation of $BaAu_3Ge$ and $CeMg_2Si_2$. The unique NTE mechanism of $SrAu_3Ge$ may also be a great playground for further theoretical studies.[15]

ASSOCIATED CONTENT

Supporting Information

The anisotropic displacement parameters for $SrAu_2Ge_2$ in Table S1, the eigenvectors for Au1, Au2, and Ge bonding bands in $SrAu_3Ge$ (Table S2), the projected partial DOS data for $SrAu_3Ge$, Figure S1, the Au 5d fatbands for $SrAu_3Ge$. Figure S2, and the cif output. This material is available free of charge via the Internet at http://pubs.acs.org.

AUTHOR INFORMATION

Corresponding Author

jcorbett@iastate.edu.

Notes

The authors declare no competing financial interest.

ACKNOWLEDGMENTS

This research was supported by the U.S. National Science Foundation, Solid State Chemistry, through grant DMR-0853732. All of the research was performed in the facilities of the Ames Laboratory, U.S. Department of Energy.

REFERENCES

(1) Lin, Q.; Corbett, J. D. *Inorg. Chem.* **2008**, *47*, 7651.
(2) Lin, Q.; Corbett, J. D. *Inorg. Chem.* **2008**, *47*, 3462.
(3) Lin, Q.; Corbett, J. D. *J. Am. Chem. Soc.* **2005**, *127*, 12786.
(4) Lin, Q.; Corbett, J. D. *J. Am. Chem. Soc.* **2007**, *129*, 6789.
(5) Lin, Q.; Corbett, J. D. *Struct. Bonding (Berlin, Ger.)* **2009**, *133*, 1.
(6) Doering, W.; Schuster, H. U. *Z. Naturforsch., B: Chem. Sci.* **1980**, *35*, 1482.
(7) Doering, W.; Schuster, H. U. *Z. Naturforsch., B: Chem. Sci.* **1979**, *34*, 1715.
(8) Laufek, F.; Vymazalová, A.; Chareev, D. A.; Kristavchuk, A. V.; Lin, Q.; Drahokoupil, J.; Vasilchikova, T. M. *J. Solid State Chem.* **2011**, *184*, 2794.
(9) Lin, Q.; Corbett, J. D., unpublished results.
(10) Lin, Q.; Corbett, J. D. *Inorg. Chem.* **2011**, *50*, 1808.
(11) Parthé, E.; Chabot, B.; Braun, H. F.; Engel, N. *Acta Crystallogr.* **1983**, *B39*, 588.
(12) Zheng, C.; Hoffmann, R. *Z. Naturforsch.* **1986**, *41b*, 292.
(13) Lin, Q.; Corbett, J. D. *Inorg. Chem.* **2009**, *48*, 5403.
(14) Evans, J. S. O.; Mary, T. A.; Vogt, T.; Subramanian, M. A.; Sleight, A. W. *Chem. Mater.* **1996**, *8*, 2809.

(15) Li, C. W.; Tang, X.; Muñoz, J. A.; Keith, J. B.; Tracy, S. J.; Abernathy, D. L.; Fultz, B. *Phys. Rev. Lett.* **2011**, *107*, 195504.
(16) Kraus, W.; Nolze, G. In *Powder Cell for Windows*. http://www.bam.de/de/service/publikationen/powder_cell.htm.
(17) Holland, T. J. B.; Redfer, S. A. T. *Miner. Mag.* **1997**, *61*, 65.
(18) *SHELXTL*, 6.10 ed.; Bruker Analytical X-ray Systems, Inc.: Madison, WI, 2000.
(19) Spek, A. L. *J. Appl. Crystallogr.* **2003**, *36*, 7.
(20) Tank, R.; Jepsen, O.; Burkhardt, A.; Andersen, O. K. TB-LMTO-ASA Program, Vers. 4.7; Max-Planck-Institut für Festkörperforschung: Stuttgart, Germany, 1994.
(21) Shriver, H. L. *The LMTO Method*; Springer-Verlag: Berlin, Germany, 1984.
(22) Jepsen, O.; Snob, M.; Linearized Band Structure Methods. In *Electronic Band-Structure and its Applications, Springer Lecture Notes*; Springer-Verlag: Berlin, Germany, 1987.
(23) Anderson, O. K.; Jepsen, O. *Phys. Rev. Lett.* **1984**, *53*, 2571.
(24) Lambrecht, W. R. L.; Andersen, O. K. *Phys. Rev. B* **1986**, *34*, 2439.
(25) Dronskowski, R.; Blöch, P. *J. Phys. Chem.* **1993**, *97*, 8617.
(26) Ren, J.; Liang, W.; Whangboo, M.-H.; *CAESAR for Windows*; Prime-Color Software, Inc., North Carolina State University: Raleigh, NC, 1998.
(27) Zeiringer, I.; Melnychenko-Koblyuk, N.; Grytsiv, A.; Bauer, E.; Giester, G.; Rogl, P. *J. Phase Equilib. Diffus.* **2011**, *32*, 115.
(28) Zmii, O. F.; Gladyshevskii, E. I. *Kristallografiya* **1970**, *15*, 939.
(29) May, N.; Schäfer, H. *Z. Naturforsch.* **1972**, *B27*, 864.
(30) The structure of $SrAu_2Ge_2$(*I*4/*mmm*) was rerefined from single crystal diffraction data. The lattice parameters are a = 4.519(2) Å, c = 10.356(4) Å. Sr and Au occupy special Wyckoff 2a(0 0 0) and 4d(0 $^1/_2$ $^1/_4$) sites, respectively, and Ge occupies a 4e [0 0 0.3796(2)] site. These are consistent with the report in ref 30.
(31) Cordero, B.; Gómez, V.; Platero-Prats, A. E.; Revés, M.; Echeverría, J.; Cremades, E.; Barragán, F.; Alvarez, S. *Dalton Trans.* **2008**, 2832.
(32) Spiekermann, A.; Hoffmann, S. D.; Kraus, F.; Fässler, T. F. *Angew. Chem., Int. Ed.* **2007**, *46*, 1638.
(33) Häussermann, U.; Amerioun, S.; Eriksson, L.; Lee, C.-S.; Miller, G. J. *J. Am. Chem. Soc.* **2001**, *124*, 4371.
(34) Villars, P.; Calvert, L. D. *Pearson's Handbook of Crystallographic Data for Intermetallic Phases*; 2nd ed.; American Society of Metals: Materials Park, OH, 1991; Vol. *1*.
(35) Todorov, E.; Sevov, S. C. *J. Solid State Chem.* **2000**, *149*, 419.
(36) Gout, D.; Barker, T. J.; Gourdon, O.; Miller, G. J. *Chem. Mater.* **2005**, *17*, 3661.
(37) Corbett, J. D. *Inorg. Chem.* **2010**, *49*, 13.
(38) Pyykkö, P. *Angew. Chem., Int. Ed.* **2004**, *43*, 4412.
(39) A coefficient of thermal expansion is defined by the equation $a = (1/L_0)(\Delta L/\Delta T)$, in which L is the instantaneous length, L_0 is an initial length, and ΔL and ΔT are changes in length referenced to the temperature at which L_0 is measured.
(40) Barrera, G. D.; Bruno, J. A. O.; Barron, T. H. K.; Allan, N. L. *J. Phys.: Condens. Matter* **2005**, *17*, R217.
(41) Mary, T. A.; Evans, J. S. O.; Vogt, T.; Sleight, A. W. *Science* **1996**, *272*, 90.
(42) Greve, B. K.; Martin, K. L.; Lee, P. L.; Chupas, P. J.; Chapman, K. W.; Wilkinson, A. P. *J. Am. Chem. Soc.* **2010**, *132*, 15496.
(43) Chatterji, T.; Henry, P. F.; Mittal, R.; Chaplot, S. L. *Phys. Rev. B* **2008**, *78*, 134105.
(44) Salvador, J. R.; Guo, F.; Hogan, T.; Kanatzidis, M. G. *Nature* **2003**, *425*, 702.
(45) Kamihara, Y.; Watanabe, T.; Hirano, M.; Hosono, H. *J. Am. Chem. Soc.* **2008**, *130*, 3296.
(46) Lumsden, M. D.; Christianson, A. D. *J. Phys.: Condens. Matter* **2010**, *22*, 203203.
(47) Mandrus, D.; Sefat, A. S.; McGuire, M. A.; Sales, B. C. *Chem. Mater.* **2010**, *22*, 715.
(48) Pauling, L.; Ewing, F. J. *Rev. Mod. Phys.* **1948**, *20*, 112.
(49) Raynor, G. V. *Prog. Metal Phys.* **1949**, *1*, 1.
(50) Ni, N.; Allred, J. M.; Chan, B. C.; Cava, R. J. *Proc. Natl. Acad. Sci. U.S.A.* **2011**, *108*, 1019.
(51) Lin, Q.; Corbett, J. D. *Inorg. Chem.* **2011**, *50*, 11091.
(52) Lin, Q.; Corbett, J. D. *Inorg. Chem.* **2011**, *50*, 1808.